

Experimental investigation of chimera states with quiescent and synchronous domains in coupled electronic oscillators

Lucia Valentina Gambuzza,¹ Arturo Buscarino,¹ Sergio Chessa,¹ Luigi Fortuna,¹ Riccardo Meucci,² and Mattia Frasca^{1,*}

¹*DIEEI, Università degli Studi di Catania, Viale A. Doria 6, 95125 Catania, Italy*

²*CNR-Istituto Nazionale di Ottica, Largo E. Fermi 6, 50125 Florence, Italy*

(Received 13 December 2013; revised manuscript received 25 June 2014; published 8 September 2014)

Chimera states, that is, dynamical regimes characterized by the existence of a symmetry-broken solution where a coherent domain and an incoherent one coexist, have been theoretically demonstrated and numerically found in networks of homogeneously coupled identical oscillators. In this work we experimentally investigate the behavior of a closed and an open chain of electronic circuits with neuron-like spiking dynamics and first neighbor connections. Experimental results show the onset of a regime that we call *chimera states with quiescent and synchronous domains*, where synchronization coexists with spatially patterned oscillation death. The whole experimental bifurcation scenario, showing how disordered states, synchronization, chimera states with quiescent and synchronous domains, and oscillatory death states emerge as coupling is varied, is presented.

DOI: [10.1103/PhysRevE.90.032905](https://doi.org/10.1103/PhysRevE.90.032905)

PACS number(s): 05.45.Xt, 05.45.Gg, 89.75.-k

I. INTRODUCTION

Many aspects of collective dynamics of coupled oscillators in natural (physical, chemical and biological) and artificial systems have been investigated, including the onset of symmetry breaking. Symmetry-broken behaviors have been found in populations of identical oscillators with homogeneous coupling and patterns characterized by a decomposition of the oscillators into one domain populated by units oscillating in synchrony and one made of desynchronized units [1]. Such states were termed in Ref. [2] as chimera states and, thereafter, found in many examples of complex systems [2–6]. All these works investigate coupled purely phase oscillators and conclude that the fundamental condition for the onset of chimera states is nonlocal coupling. Examples of the structures of the chimera states observed in nonlocally coupled phase oscillators include the appearance of a coherent group of phase-locked oscillators next to an incoherent domain of phase-randomized oscillators in one-dimensional rings [1,2], spiral waves with an incoherent core of phase-randomized oscillators and an arm of phase-locked units in two-dimensional systems [3–5], and the onset of a population displaying synchronized oscillations and another displaying incoherent oscillations, in a system formed by a pair of populations [6]. In the latter case the configuration is such that each oscillator is equally coupled to all the others in its group, and less strongly to those in the other group.

Recent studies have pointed out that chimera states also appear in groups of oscillators where the amplitude dynamics is not neglected [7–11]. For these oscillators the condition of nonlocal coupling is not strictly needed, and chimera states also appear in globally coupled systems [8,10] or in one-dimensional arrays with nearest neighbor coupling [11]. In such systems chimera states with different structures have been observed, and, consequently, several terms have been used to refer to these phenomena. The term *amplitude-mediated chimera* has been used to refer to chimera states that, with respect to their counterpart in purely phase oscillators, also

display temporal variations of the amplitude in the incoherent population [7]. A chimera behavior of the oscillator amplitude, rather than its phase, and named a *amplitude chimera state* has been instead reported in Ref. [9], which also shows *chimera death states*, that is, regimes characterized by coexistence of spatially coherent and incoherent oscillation death. Finally, another type of chimera state appearing as a pattern where a group of synchronized units coexist with an incoherent domain of units undergoing a spatially patterned oscillation death (SPOD) regime is reported in Ref. [11]. Our analysis refers to this latter type of chimera states, and, to distinguish them from the other chimera structures reported in literature, we refer to them as *chimera states with quiescent and synchronous domains* (QSCS). A peculiarity of the system under investigation is that a population of neurons is considered, which is important, keeping in mind that chimera states have been suggested to be in a relation with the phenomenon of uni-hemispheric sleep, characterized by desynchronized electrical activities in the awake side of the brain and synchronized in the sleeping side [6]. The new chimera state observed shows the coexistence of the two characteristic regimes of neuronal activity of a FHN neuron, that is, the quiescent state and the oscillatory regime. We also mention that, in populations of neurons, multichimera states, namely, chimera states with more than one incoherent domain, have been observed in Ref. [12], and they have also been found in our experiments.

Despite the abundance of closed-form solvable models and numerical evidences of chimera states, only a few experimental studies have been carried out. Experiments in nonlinear optics have revealed chimera states in a liquid-crystal spatial light modulator [13]. The system represents a spatially extended iterated map, where coupling and feedback are controlled by a computer. Chimera states appear both in 1D and 2D lattice configurations. Populations of chemical oscillators coupled through feedback signals (controlled light intensity conditions) were investigated in Ref. [14]. These experiments, in particular, were performed with coupled Belousov-Zhabotinsky oscillators and also showed unexpected chimera behaviors such as phase-cluster states. A totally analog experiment was instead devised in Ref. [15], where a hierarchical network of

*mfrasca@dieei.unict.it

coupled mechanical oscillators was realized. The experimental setup consists of a set of metronomes placed on two swings free to move in a plane: within each swing the oscillators are strongly coupled by the motion of the support, while springs between the two swings implement the weak coupling between the two oscillator subpopulations. A further case study is reported in Ref. [16] where a single Ikeda time-delayed system is implemented to experimentally prove the onset of virtual chimera states, that is, the coexistence of synchronous and incoherent oscillations in a virtual space-time representation.

In our work we experimentally investigate the onset of chimera states in a system of coupled electronic oscillators. Each oscillator mimics the dynamics of a FitzHugh-Nagumo (FHN) neuron and is coupled with its nearest neighbors in a chain configuration (we consider either a closed or an open chain). The proposed system is totally analog and does not require any external control, so that chimera states appear without any fine-tuning of both the coupling and oscillator parameters. We first discuss the appearance of QSCS in a ring configuration and, then, show that this new type of chimera state can also exist in an open chain configuration.

II. EXPERIMENTAL SETUP

The core of the experimental setup is an electronic circuit implementing the dynamics of a FHN neuron designed and realized with off-the-shelf components [17]. The experiments have been carried out on $N = 10$ circuits coupled in a chain configuration, where each circuit is coupled with its nearest neighbors.

The dimensionless equations describing the FHN neuron [17] are

$$\begin{aligned} \frac{dx_i}{d\tau} &= x_i - y_i - ax_i^3 \\ \frac{dy_i}{d\tau} &= \varepsilon(x_i - by_i + c + f_i), \end{aligned} \quad (1)$$

where x_i and y_i are the fast and the recovery variable of neuron i , with $i = 1, \dots, N$, τ represents time, and a, b, c are parameters governing the single-neuron dynamics. The term f_i is the coupling of neuron i with neurons $i - 1$ and $i + 1$ and is given by

$$f_i = D(y_{i-1} + y_{i+1} - 2y_i) \quad i = 1, \dots, N \quad (2)$$

for the closed chain (ring configuration) and by

$$f_i = \begin{cases} D(y_{i+1} - y_i) & i = 1 \\ D(y_{i-1} + y_{i+1} - 2y_i) & i = 2, \dots, N - 1 \\ D(y_{i-1} - y_i) & i = N \end{cases} \quad (3)$$

$$F_i = \begin{cases} R_c \left(\frac{1}{R_{19}} Y_{i+1} - \frac{1}{R_{20}} \frac{R_{17}}{R_{16}} Y_i \right) & i = 1 \\ R_c \left(\frac{1}{R_{18}} Y_{i-1} + \frac{1}{R_{19}} Y_{i+1} - \frac{1}{R_{20}} \frac{R_{17}}{R_{16}} Y_i \right) & i = 2, \dots, N - 1 \\ R_c \left(\frac{1}{R_{18}} Y_{i-1} - \frac{1}{R_{20}} \frac{R_{17}}{R_{16}} Y_i \right) & i = N \end{cases} \quad (6)$$

for the open chain.

for the open chain. The parameter D represents the coupling coefficient. In Eqs. (1) the diffusive coupling involves the recovery variable; we have determined that the diffusion of the fast variable [x_i in Eqs. (1)] leads to only two regimes (unsynchronized or synchronized behavior) depending on the coupling strength. Therefore, our analysis in the following is limited to coupling as in Eqs. (1).

In our electronic implementation of Eqs. (1) each state variable is associated with the voltage across a capacitor, and operational amplifiers and analog multipliers are used to implement the mathematical operations in the model. The design follows a standard approach for nonlinear circuit implementations [18]. In particular, at first, rescaled variables $X_i = \frac{x_i}{2} V_0$ and $Y_i = y_i V_0$ with $V_0 = 1$ V are introduced, so that the signals in the circuit do not overcome the power supply values, which in our case have been fixed to ± 12 V.

The scheme adopted for one FHN circuit and the coupling circuitry are reported in Fig. 1. The nonlinearity has been realized with two AD633 analog multipliers whose input-output relation is given by $W = (I_1 - I_2)(I_3 - I_4)/V_1 + Z$ with $V_1 = 10$ V (V_1 is a scaling reference of the multiplier). In the circuit, for the first multiplier, we fixed $I_2 = I_4 = 0$ and $Z_1 = \frac{R_4}{R_3 + R_4} W_1$, so that $W_1 = \frac{I_1 I_3}{V_1} \frac{R_3 + R_4}{R_3}$. Analogously, in the second multiplier $W_2 = \frac{I_1 I_3}{V_1} \frac{R_1 + R_2}{R_1}$.

The equations governing each FHN circuit are

$$\begin{aligned} \frac{dX_i}{dt} &= \frac{1}{R_7 C_1} \left(X_i - \frac{R_7}{R_9} Y_i - \frac{R_7}{R_8} \frac{R_1 + R_2}{V_1 R_1} \frac{R_3 + R_4}{V_1 R_3} X_i^3 \right) \\ \frac{dY_i}{dt} &= \frac{1}{R_7 C_2} \left(\frac{R_7}{R_{13}} X_i - \frac{R_7}{R_{10}} Y_i - \frac{R_7}{R_{12}} \frac{R_{15}}{R_{14} + R_{15}} V_- \right. \\ &\quad \left. + \frac{R_7}{R_{11}} F_i \right). \end{aligned} \quad (4)$$

In deriving these equations we have implicitly assumed that $R_5 = R_6$, so that the operational amplifier U2 is an inverting stage with gain equal to -1 , and that the resistor R_{12} is much larger than R_{14} (that is, R_{14} and R_{15} work as a voltage divider). The term F_i represents the coupling of circuit i with circuits $i - 1$ and $i + 1$; it is given by

$$F_i = R_c \left(\frac{1}{R_{18}} Y_{i-1} + \frac{1}{R_{19}} Y_{i+1} - \frac{1}{R_{20}} \frac{R_{17}}{R_{16}} Y_i \right) \quad i = 1, \dots, N \quad (5)$$

for the closed chain (ring configuration) and by

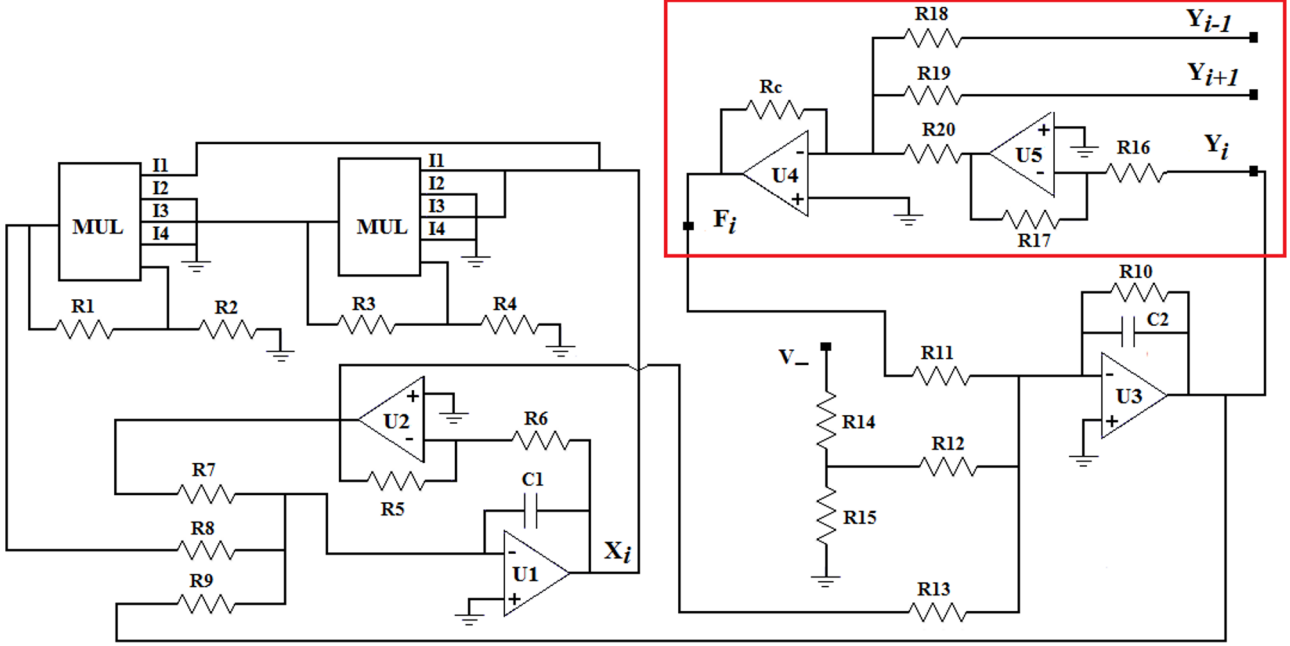


FIG. 1. (Color online) Schemes of the FHN circuit including the coupling circuitry (in the red box). The following component values have been used: $R_1 = 1 \text{ k}\Omega$, $R_2 = 10 \text{ k}\Omega$, $R_3 = 1 \text{ k}\Omega$, $R_4 = 10 \text{ k}\Omega$, $R_5 = 1 \text{ k}\Omega$, $R_6 = 1 \text{ k}\Omega$, $R_7 = 100 \text{ k}\Omega$, $R_8 = 75 \text{ k}\Omega$, $R_9 = 200 \text{ k}\Omega$, $R_{10} = 123 \text{ k}\Omega$, $R_{11} = 100 \text{ k}\Omega$, $R_{12} = 330 \text{ k}\Omega$, $R_{13} = 50 \text{ k}\Omega$, $R_{14} = 11 \text{ k}\Omega$, $R_{15} = 1.1 \text{ k}\Omega$, $R_{16} = 1 \text{ k}\Omega$, $R_{17} = 1 \text{ k}\Omega$, $R_{18} = 10 \text{ k}\Omega$, $R_{19} = 10 \text{ k}\Omega$, $C_1 = 3.3 \text{ nF}$, $C_2 = 39 \text{ nF}$. AD633 analog multipliers and TL084 have been used as integrated devices. The power supply is $V_+ = 12 \text{ V}$ and $V_- = -12 \text{ V}$. In the open chain setup, R_{18} for FHN 1 and R_{19} for FHN 10 are not used as the first and the tenth FHN are not connected to each other. Moreover, in the open chain setup $R_{20} = 5 \text{ k}\Omega$ for neuron i with $i = 2, \dots, N-1$ and $R_{20} = 10 \text{ k}\Omega$ for $i = \{1, N\}$, while in the closed chain setup $R_{20} = 5 \text{ k}\Omega$ for all neurons.

The circuit equations (4) match the model equations (1) for $X_i = \frac{x_i}{2} V_0$ and $Y_i = y_i V_0$ and $t = \kappa \tau$ (where $\kappa = R_7 C_1 = 3.3 \times 10^{-4} \text{ s}$ introduces a rescaling in the time axis), and for the following relationships between the model parameters and the circuit components:

$$\begin{aligned}
 \varepsilon &= \frac{C_1}{C_2} \\
 a &= \frac{1}{4} \frac{R_7}{R_8} \frac{R_1 + R_2}{V_1 R_1} \frac{R_3 + R_4}{V_1 R_3} V_0^2 \\
 b &= \frac{R_7}{R_{10}} \\
 c &= -\frac{R_7}{R_{12}} \frac{R_{15}}{R_{14} + R_{15}} \frac{V_-}{V_0} \\
 D &= \frac{R_7}{R_{11}} \frac{R_c}{R},
 \end{aligned} \tag{7}$$

where in the expression of D we have taken into account that $R = R_{18} = R_{19}$. The ring and the open chain configurations differ for the connection of the first and last FHN circuit. In the ring setup the first and the last circuit are connected, so that each FHN circuit has the same coupling circuitry with $R = R_{18} = R_{19} = 2R_{20}$. When the open chain is investigated, the first and the last circuit are not connected each other, and the resistances of the coupling circuitry are recalculated to match the mathematical model. This means to choose for the first FHN circuit $R_{18} = 0$ and $R = R_{20} = R_{19}$, for the FHN

circuit from $i = 2$ to $i = N-1$ $R = R_{18} = R_{19} = 2R_{20}$, and for the last FHN circuit $R_{19} = 0$ and $R = R_{20} = R_{18}$.

In our experiments, the model parameters are fixed as $\varepsilon = 0.085$, $a = 0.4$, $b = 0.8$, $c = 0.33$, and, correspondingly, the component values as reported in the caption of Fig. 1. For these parameters the single uncoupled FHN circuit exhibits the periodic oscillations shown in Fig. 2. The oscillation frequency of signals reported in Fig. 2 is about 81.3 Hz. In our implementation 5% precision off-the-shelf components have been used; due to these component tolerances, the oscillation frequency varies from neuron to neuron with a nominal value of 76 Hz and a 10% precision. The coupling coefficient is experimentally controlled by the resistor R_c , which has been varied from 0 to 10 k Ω , and corresponds to parameter D in the range [0, 1].

III. ANALYSIS

The experimental setup described in Sec. II was operated in a totally analog way, by manually (and simultaneously for each FHN circuit) varying the coupling resistors R_c , to run experiments at different coupling values. We start our discussion by considering the ring setup.

Several dynamical regimes have been identified in the system: a disordered state where all neurons oscillate independently and with their own phase; a regime of phase synchronization of all the FHN units, where all frequencies are locked and the phase differences between units remain constant in time; a SPOD regime, that is a regime, where

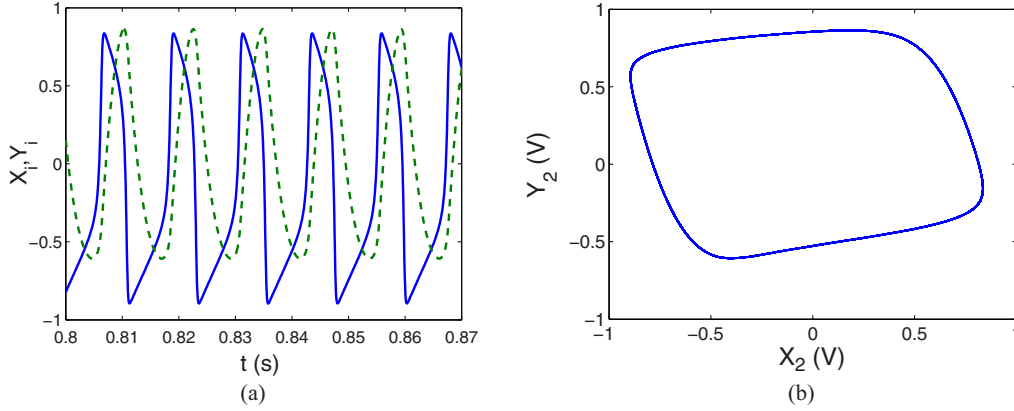


FIG. 2. (Color online) Behavior of a single uncoupled FHN circuit (in particular, circuit 2). (a) Trend of the variables X (solid blue line) and Y (dashed green line). The x -axis unit is expressed in seconds. (b) Plane X - Y . The signals are acquired with a sampling frequency equal to $f_s = 15$ kHz.

all the neurons reach a steady state, which, however, varies from neuron to neuron forming an inhomogeneous pattern; and QSCS, where coherent oscillations in a part of the ring coexist with a spatially patterned stationary state for a subset of the neurons. As in many other systems showing chimera states, the appearance of a given dynamical regime is a function of the coupling. One important finding is that, for the same coupling strength but different set of initial conditions, more than one dynamical state are simultaneously possible and stable (for the same value of the coupling either the phase synchronized state

and QSCS or SPOD and QSCS are observed), and, in addition, different patterns of the same type (e.g., SPOD or QSCS) have been found.

When coupling is varied, usually the probability of finding one state rather than another changes. In our experiments, for zero or low coupling the disordered state appears with oscillators running at their own frequency [Fig. 3(a) and Fig. 4(a)], which as mentioned above is slightly different from neuron to neuron. When coupling is increased, neurons become phase synchronized [Fig. 3(b) and Fig. 4(b)]. Higher values of

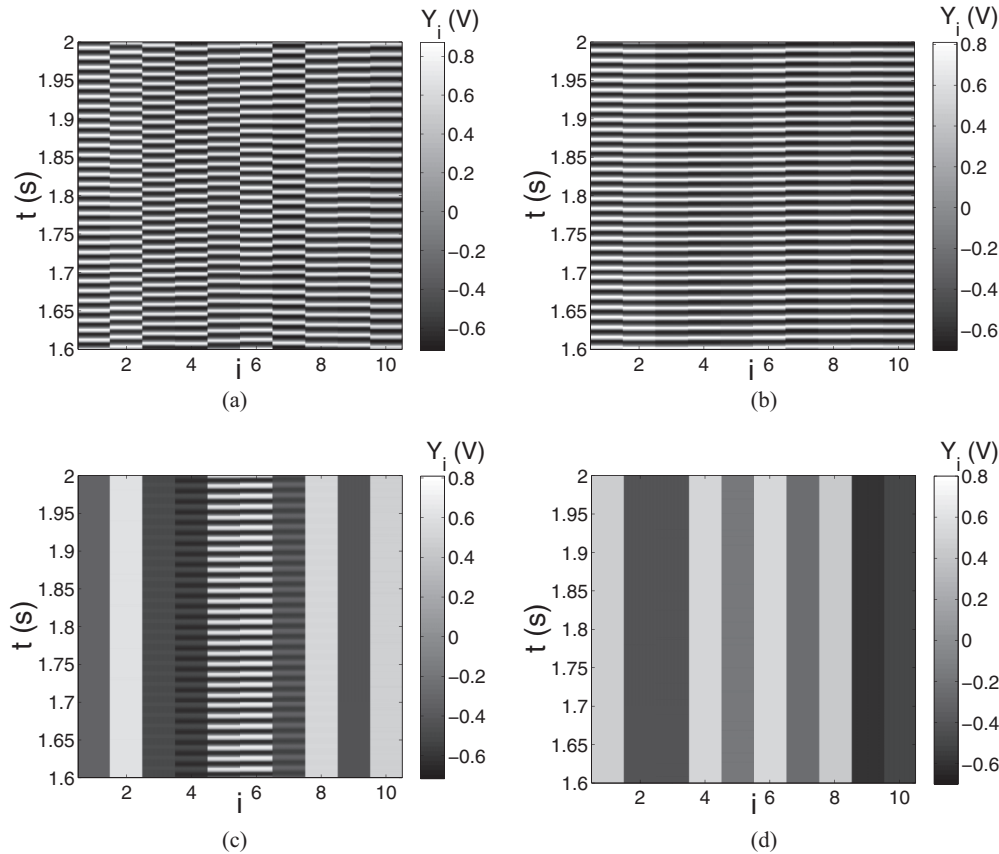


FIG. 3. Experimental spatiotemporal behavior of the ring of $N = 10$ FHN circuits at different values of the coupling coefficient: (a) unsynchronized oscillations, $D = 0$; (b) phase synchronized oscillations, $D = 0.3$; (c) QSCS, $D = 0.5$; (d) SPOD, $D = 0.675$.

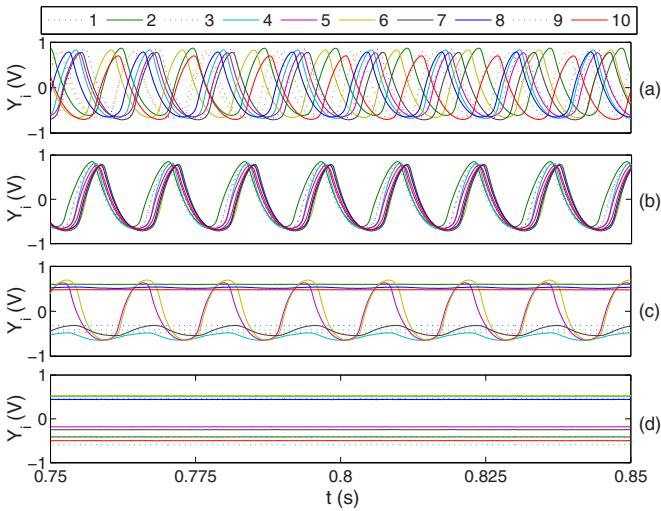


FIG. 4. (Color online) Trend of the state variable Y_i for the four dynamical states observed as in Fig. 3: (a) unsynchronized oscillations, $D = 0$; (b) phase-synchronized oscillations, $D = 0.3$; (c) QSCS, $D = 0.5$; (d) SPOD, $D = 0.675$.

coupling lead to the appearance of QSCS [Fig. 3(c) and Fig. 4(c)], where oscillating neurons coexist with neurons exhibiting almost stationary states, and to SPOD states [Fig. 3(d) and Fig. 4(d)], where all the neurons are at a space-dependent steady state. After that, the SPOD regime

is maintained, even if the coupling is further increased. These regimes are also confirmed by numerical simulations of Eqs. (5) and (1) (see Fig. S7 in the Supplemental Material [19]).

Referring to the experimental results of Fig. 3(c), it is interesting to note that in chimera-like states, contrarily to partial synchronization, the oscillators forming the coherent group are not those having the closest natural frequencies. In fact, oscillators 5 and 6 are phase synchronized, but their natural frequencies are 78.86 Hz and 81.44 Hz, while that of oscillator 4 is 78.52 Hz.

We have experimentally verified that, when D is fixed so that QSCS are found, distinct patterns are simultaneously possible. The patterns typically differ for the composition of the coherent and incoherent domain (number of units belonging to each domain, position of the domain in the chain), which is a function of the initial conditions. An example is shown in Fig. 5 where two different QSCS and two SPOD at $D = 0.575$ are shown. Different initial conditions have been simply obtained by turning off and then on again the power supply; therefore, they are totally random and not controllable. Several other examples have been registered [19] (Figs. S1–S3 show experimental results illustrating this finding, and Figs. S4–S6 the corresponding numerical simulations). The same consideration holds for SPOD, where patterns differing for the specific value of the steady state reached by each neuron may be observed at the same value of D , provided that they respect the symmetry of the system.

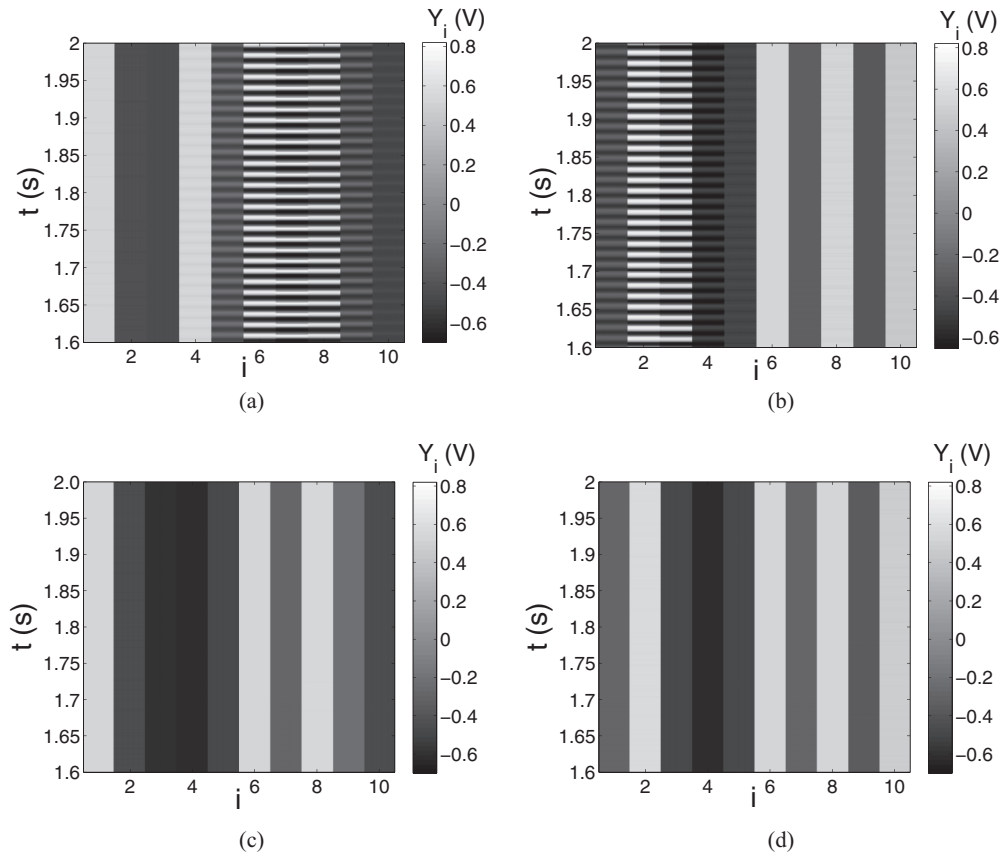


FIG. 5. (a)–(b) Two chimera states; (c)–(d) two SPOD obtained in the ring for different initial conditions at the same value of the coupling coefficient D ($D = 0.575$).

For a more systematic characterization of the system behavior, we have performed a set of acquisitions by varying R_c from $0\ \Omega$ to $10\ \text{k}\Omega$ at steps of $250\ \Omega$, which corresponds to change D from 0 to 1 at steps of 0.025. For each value of the coupling coefficient, we have registered 20 different acquisitions, each time by switching off the power supply, waiting for 3–4 s and then turning on the power supply and registering the data. Data, in particular the waveform of the Y_i variable for all the circuits, have been acquired by using an acquisition board (National Instruments NI-USB6255) with a sampling frequency of 15 kHz, and recording 50 000 samples for each acquisition. The protocol, aimed at registering the results of different initial conditions for each value of the coupling, has been thus repeated for 41 values in the interval from $R_c = 0\ \Omega$ to $R_c = 10\ \text{k}\Omega$ (D from $D = 0$ to $D = 1$), so that for all 820 acquisitions have been done for each set.

The distinct regimes have been classified by monitoring the temporal variance of Y_i , $\sigma_t^2(Y_i)$ as in Ref. [11] and the Kuramoto order parameter defined below. The first parameter is used to classify the neurons as oscillating or not, with low values of $\sigma_t^2(Y_i)$ indicating neurons at a steady state. Based on this, the number of nonoscillating neurons N_{no} is defined and SPOD states are identified as regimes with $N_{\text{no}} = N$, while chimera as states with $0 < N_{\text{no}} < N$.

When $N_{\text{no}} = 0$, all the neurons are oscillating. To evaluate their level of phase synchronization, we use the Kuramoto order parameter computed as follows. For each acquired signals Y_i , the following phase variable is defined:

$$\theta(t) = 2\pi \left(k + \frac{t - \tau_k}{\tau_{k+1} - \tau_k} \right) \quad (8)$$

where τ_k is the peak time. The Kuramoto order parameter $r_{nm} = \langle |e^{i[\theta_n(t) - \theta_m(t)]}| \rangle_t$ is then calculated to monitor phase synchronization between circuit n and circuit m , and, the global level of synchronization of the system is evaluated by averaging r_{nm} among all the possible pairs of circuits, that is,

$$r = \frac{1}{N(N-1)} \sum_{n,m=1;n \neq m}^N r_{nm}. \quad (9)$$

Oscillators are synchronized when $r > 0.8$. The complete experimental characterization of the system behavior is reported in Fig. 6. The characterization is performed with respect to the coupling coefficient D , derived as $D = \frac{R_c}{R}$. For each value of D we report the percentage of states classified as phase synchronized (PS), unsynchronized (US), QSCS, and SPOD.

When D is low, the system is not synchronized. Synchronized oscillations are observed starting from $D \geq 0.2$. QSCS systematically appear in the range of D from 0.4 to 0.6, which corresponds to R_c varying from $R_c = 4000\ \Omega$ to $R_c = 6000\ \Omega$. For $D \in [0.6, 1]$ the regime is mostly characterized by SPOD states.

The analysis of Fig. 6 confirms that two or more dynamical states of the same type (that is, two or more QSCS for instance) or of different types (a synchronous state and a QSCS, for instance) may coexist at the same values of the coupling and, in general, the regions in which the specific dynamical states appear overlap. For example, for $D = 0.425$ either synchronous states or QSCS, depending on initial conditions,

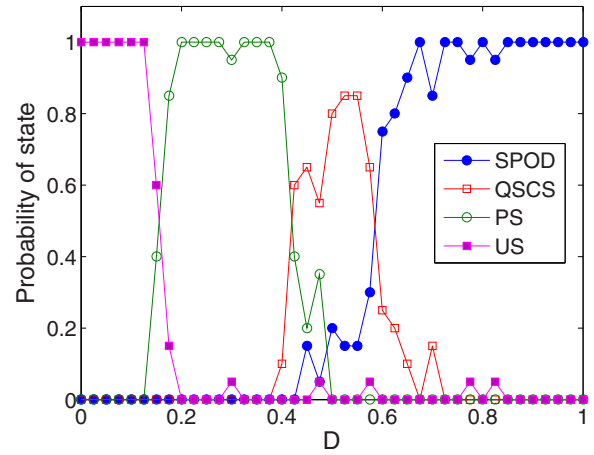


FIG. 6. (Color online) Probability of states for the closed chain (ring) of $N = 10$ FHN circuits with respect to the value of the coupling coefficient D . For each value of D , 20 different acquisitions have been performed, and the percentage of states classified as SPOD, QSCS, PS, or unsynchronized states (US) is reported. As coupling is increased, the system behavior changes from a disordered state to synchronization, QSCS, and SPOD.

are found, while for $D \in [0.425, 0.725]$ QSCS and SPOD with different probability along the range are observed.

The set of acquisitions from $D = 0$ to $D = 1$ has been repeated several times by exchanging the position of some circuits in the ring, in order to investigate the effect of circuit tolerances. The result is that the qualitative behavior of the system is robust to such changes. In all of these experiments the four dynamical regimes (unsynchronized state, phase synchronization, QSCS, and SPOD) have been observed in the same order, although the transition from one dynamical regime to another one may be shifted left or right. Furthermore, from

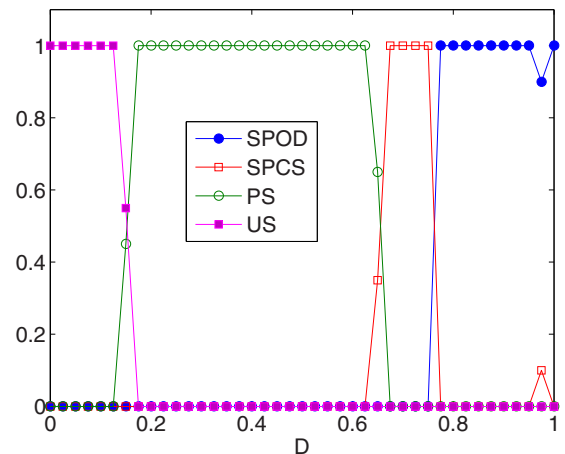


FIG. 7. (Color online) Probability of the states for the open chain of $N = 10$ FHN circuits with respect to the value of the coupling coefficient D . For each value of D , 20 different acquisitions have been performed and the percentage of states classified as SPOD, QSCS, PS, or unsynchronized states (US) is reported. As coupling is increased, the system behaviors changes from a disordered state to synchronization, QSCS, and SPOD.

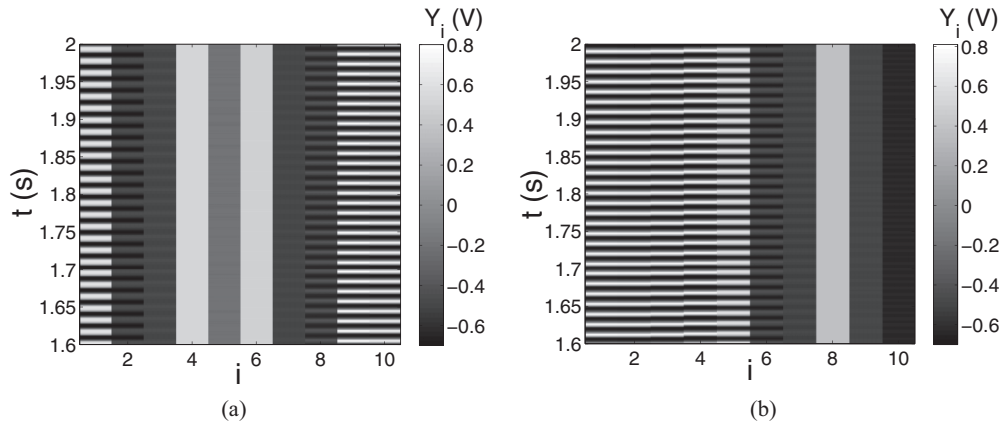


FIG. 8. Two chimera states obtained in the open chain for different initial conditions at the same value of the coupling coefficient D ($D = 0.7$).

one acquisition set to another the observed QSCS differ for the composition of the coherent and incoherent domain. The mechanism leading to chimera states as well as to SPOD states is driven by symmetry breaking: in our circuits it is influenced by the component tolerances, so that the general feature of the phenomenon are preserved but the specific patterns observed vary from one acquisition set to another.

To further investigate this new type of chimera states, an open chain configuration of $N = 10$ FHN circuits has been also implemented and characterized. The experimental setup has been realized by disconnecting the last neuron (circuit 10) to the first neuron of the chain (circuit 1) and rearranging the resistances of the coupling circuitry as described in Sec. II. The behavior of the system has been studied by monitoring the same measures used for the ring under the same operating conditions (20 different acquisitions for each value of D , varied in the range $[0, 1]$ at steps of 0.025). The experimental characterization of the open chain configuration is reported in Fig. 7.

Also in this case, QSCS appear in a region of the parameter space between those of synchronized and SPOD behavior. In particular, two examples of QSCS obtained for the same value of D ($D = 0.7$), but different initial conditions (obtained by turning off and then on again the power supply), are reported in

Fig. 8. We notice that the state reported in Fig. 8(a) actually is a multichimera state as the units are split into three domains: two coherent close to the boundaries and one incoherent in the middle of the array. Another example of simultaneously possible QSCS is reported in Fig. S8 [19], along with the corresponding numerical simulations shown in Fig. S9.

The comparison of the experimental results obtained with the closed and the open chain configuration clearly shows that the boundary conditions do not impact the onset of the dynamical regimes that can be observed, as all the four states are found in both setups. The phenomenon of coexistence between different dynamical regimes is more evident when the two extreme FHN circuits are connected: we attribute this to the different basins of attractions of the dynamical states in the closed and in the open chain.

To investigate size effects, we have numerically studied the closed and the open chain with a larger number of FHN units. N has been increased up to 1000, while monitoring the percentage of QSCS (over 20 initial conditions) as a function of the coupling coefficient D . The results are reported in Fig. 9, which shows that the region of QSCS is independent from the system size. However, as the system size increases, the probability of QSCS is higher, that is, at a given value of coupling, the occurrence of QSCS increases for larger systems.

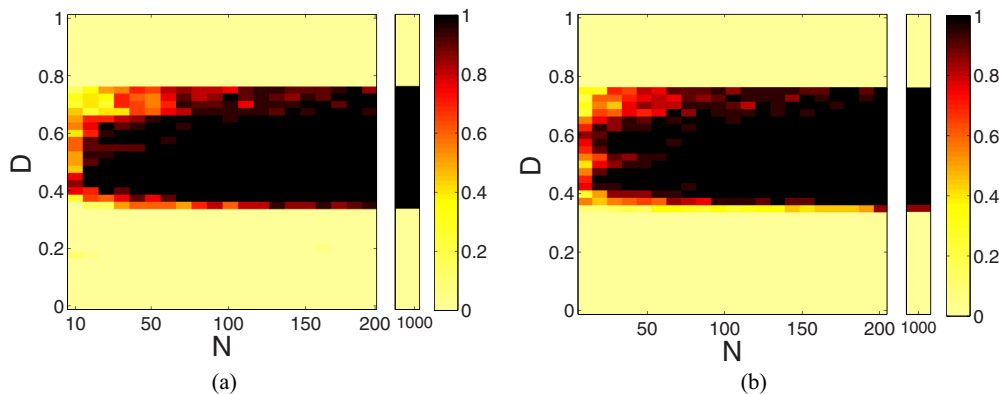


FIG. 9. (Color online) Occurrence of QSCS for the closed (a) and open chain (b) of FHN neurons with different sizes N as function of the coupling coefficient D . For each value of D and N , 20 simulations, starting from different initial conditions, have been considered, and the percentage of QSCS over these runs is reported.

IV. CONCLUSIONS

The abundance of theoretical and numerical studies on chimera states calls for experimental investigations of such states on real systems. In this work we have proposed a totally analog system of coupled electronic oscillators exhibiting chimera states with quiescent and synchronous domains. The proposed system does not require any external control by computers or other digital processors: coupling is varied through resistors, and then experiments at different coupling values are performed. The results allow to conclude that chimera states appear without any fine-tuning of both the coupling and oscillator parameters. Furthermore, we have found that these states are quite robust to the boundary

conditions (both closed and open chain configurations have been investigated) and to the system size. The emergence of chimera states with quiescent and synchronous domains has been also found in different sets of acquisitions where the position of the circuits in the chain was varied (so varying the asymmetries due to component tolerances), although the specific pattern observed depends on the circuit position.

ACKNOWLEDGMENT

The authors would like to thank Stefano Euzzor for his suggestions and comments.

-
- [1] Y. Kuramoto and D. Battogtokh, *Nonlinear Phenom. Complex Syst.* **5**, 380 (2002).
 - [2] D. M. Abrams and S. H. Strogatz, *Phys. Rev. Lett.* **93**, 174102 (2004).
 - [3] S.-I. Shima and Y. Kuramoto, *Phys. Rev. E* **69**, 036213 (2004).
 - [4] E. A. Martens, C. R. Laing, and S. H. Strogatz, *Phys. Rev. Lett.* **104**, 044101 (2010).
 - [5] A. E. Motter, *Nat. Phys.* **6**, 164 (2010).
 - [6] D. M. Abrams, R. Mirollo, S. H. Strogatz, and D. A. Wiley, *Phys. Rev. Lett.* **101**, 084103 (2008).
 - [7] G. C. Sethia, A. Sen, and G. L. Johnston, *Phys. Rev. E* **88**, 042917 (2013).
 - [8] L. Schmidt, K. Schonleber, K. Krischer, and V. Garcia-Morales, *Chaos* **24**, 013102 (2014).
 - [9] A. Zakharova, M. Kapeller, and E. Schöll, *Phys. Rev. Lett.* **112**, 154101 (2014).
 - [10] G. C. Sethia and A. Sen, *Phys. Rev. Lett.* **112**, 144101 (2014).
 - [11] R. Singh and S. Sinha, *Phys. Rev. E* **87**, 012907 (2013).
 - [12] I. Omelchenko, O. E. Omel'chenko, P. Hövel, and E. Schöll, *Phys. Rev. Lett.* **110**, 224101 (2013).
 - [13] A. M. Hagerstrom, T. E. Murphy, R. Roy, P. Hovel, I. Omelchenko, and E. Scholl, *Nat. Phys.* **8**, 658 (2012).
 - [14] M. R. Tinsley, S. Nkomo, and K. Showalter, *Nat. Phys.* **8**, 662 (2012).
 - [15] E. A. Martens, S. Thutupalli, A. Fourriere, and O. Hallatschek, *Proc. Natl. Acad. Sci. USA* **110**, 10563 (2013).
 - [16] L. Larger, B. Penkovsky, and Y. Maistrenko, *Phys. Rev. Lett.* **111**, 054103 (2013).
 - [17] M. Ciszak, S. Euzzor, F. T. Arecchi, and R. Meucci, *Phys. Rev. E* **87**, 022919 (2013).
 - [18] L. Fortuna, M. Frasca, and M. G. Xibilia, *Chua's Circuit Implementations: Yesterday, Today and Tomorrow* (World Scientific, Singapore, 2009).
 - [19] See Supplemental Material at <http://link.aps.org/supplemental/10.1103/PhysRevE.90.032905> for more experimental and numerical results.